ACI STRUCTURAL JOURNAL TECHNICAL PAPER

Title no. 96-S21

Towards Cyclic Load Modeling of Reinforced Concrete

by F. J. Vecchio

Formulations are presented by which a secant stiffness-based finite element algorithm can be modified to provide analysis capability for arbitrary loading conditions, including reversed cyclic loads. Plastic offset strains are defined for concrete and reinforcement, and these are incorporated into the analysis through the use of prestrain forces. The elastic components of strain are then used to define effective secant stiffness factors. To provide a record of plastic offsets, and of maximum strain experienced during previous loading, strain envelopes are defined using a Mohr's circle construction. Provisional constitutive models are presented for the concrete, although further work is required in this area. An analysis of a shearwall shows the procedure to be stable and compliant and to provide reasonably accurate simulations of behavior. The results of a pilot series of panel tests are used to identify the aspects of concrete modeling that are in need of further study and refinement.

Keywords: cyclic loads; models; reinforced concrete; shear tests.

INTRODUCTION

In the analysis of reinforced concrete structures, a number of diverse approaches have been used for material modeling. These include plasticity-based procedures, fracture mechanics procedures, and various nonlinear elastic models. In the latter case, approaches range from discrete crack models to smeared crack models, and from fixed crack models to rotating crack models. Researchers working in each of these areas generally have been successful in producing models that yield results of acceptable accuracy for conditions of monotonic loading. These efforts are well-documented in the literature.[1]

Models that provide accurate simulations of behavior under general loading conditions, and specifically under reversed cyclic loading, are somewhat less common. For such formulations, the smeared crack approach tends to be the most favored. Okamura and Maekawa[2] and Sittipunt and Wood,[3] among others, have documented models assuming fixed cracks directions and have demonstrated good correlation to experimental results. In some fixed crack formulations, separate models have been used to model the normal stress and shear stress hysteretic behaviors. This is somewhat at odds both with the test observations and with common elasticity approaches to constitutive modeling. Stevens et al.[4] used a more comprehensive constitutive modeling approach for concrete in a rotating smeared crack content. However, the tangent stiffness procedure used by Stevens resulted in some numerical difficulties under cyclic load conditions.

An alternative approach previously described was also based on the smeared rotating crack assumption.[5,6] The procedure was based on an iterative, secant stiffness formulation treating concrete as an orthotropic material modeled according to the constitutive relations of the modified compression field theory.[7] The secant stiffness formulation resulted in a procedure marked by excellent convergence and numerical stability characteristics. Correlations to experimental data, for structures subjected to monotonic loading conditions, were generally very good. However, a criticism of the secant stiffness approach has been that it cannot be effectively used to model response to general loading.

Presented herein are formulations whereby a secant stiffness-based algorithm, employing the smeared rotating crack assumption, can be adapted to represent hysteretic material response under general and reserved cyclic loading. The computational advantages of the secant stiffness approach are retained without any compromise to the material behavior models that can be used. The need to separate shear and normal in-plane behavior is also eliminated.

RESEARCH SIGNIFICANCE

The need for accurate methods of analysis of reinforced concrete structures under general loading conditions has been brought to the fore by structural failures sustained during the recent Northridge and Kobe earthquakes. Many of the collapses involved structural elements subjected to lateral shears, placing high strength and ductility demands on the cracked reinforced concrete. Current ability to model response under such conditions is not well-advanced.

This paper presents an alternative method by which finite element analysis procedures can be made to provide accurate simulations of reinforced concrete subjected to reversed cyclic loads. Emphasis is placed on developing simple, numerically stable formulations. The analysis of a shearwall structure, and the results of a pilot test program, are also presented in a discussion of the importance of proper constitutive modeling.

PLASTIC OFFSET FORMULATION

Consider the stress and strain conditions in a concrete element previously subjected to an arbitrary load history. Suppose that at a particular point in time, in a principal strain direction, the stress and total strain in the concrete are f_{c1} and ε_{c1}, respectively, as shown in Fig. 1. The total strain can be considered to consist of an elastic strain component ε_c^e and a plastic strain component (or plastic offset) ε_c^p; thus

$$\varepsilon_c = \varepsilon_c^e + \varepsilon_c^p \tag{1}$$

The elastic strain can then be used to compute an effective secant stiffness for the concrete

$$\bar{E}_c = \frac{f_c}{\varepsilon_c^e} \tag{2}$$

However, the plastic strain must then be treated as a strain offset, similar to elastic offsets resulting from thermal expansion, shrinkage, or other prestrain effects.

Formulations were previously described in References 6 and 8, whereby elastic prestrains were rigorously incorporated into a finite element algorithm based on a smeared, rotating crack model and a secant stiffness approach. The plastic offsets can

ACI Structural Journal, V. 96, No. 2, March-April 1999.
Received January 8, 1997, and reviewed under Institute publication policies. Pertinent discussion will be published in the January-February 2000 *ACI Structural Journal* if received by September 1, 1999.

F. J. Vecchio, *FACI, is a professor of civil engineering at the University of Toronto. He is a member of Joint ACI-ASCE Committees 441, Reinforced Concrete Columns, and 447, Finite Element Analysis of Reinforced Concrete Structures. His research interests include constitutive modeling, nonlinear analysis, and rehabilitation of structures.*

be accommodated in an analogous manner. To do so, the plastic offsets in the principal directions are first resolved into components relative to the reference axes, giving the vector $[\varepsilon_c^p]$

$$[\varepsilon_c^p] = \begin{bmatrix} \varepsilon_{cx}^p \\ \varepsilon_{cy}^p \\ \gamma_{cxy}^p \end{bmatrix} \tag{3}$$

From the prestrains, free joint displacements are determined as functions of the element geometry. Then, given the free displacements, the plastic prestrain nodal forces can be evaluated using the effective element stiffness matrix due to the concrete component (see Reference 6 for details).

The plastic offsets developed in each of the reinforcement components are handled in a similar manner. For a reinforcement component oriented in direction α_i, having a plastic offset of $\varepsilon_{s_i}^p$, the prestrain matrix is

$$[\varepsilon_s^p]_i = \begin{bmatrix} \varepsilon_{s_i}^p \cdot (1 + \cos 2\alpha_i)/2 \\ \varepsilon_{s_i}^p \cdot (1 - \cos 2\alpha_i)/2 \\ \varepsilon_{s_i}^p \cdot \sin 2\alpha_i \end{bmatrix} \tag{4}$$

The corresponding plastic prestrain nodal forces are then determined accordingly. At the same time, the secant stiffness for the reinforcement must be calculated as

$$\bar{E}_{s_i} = \frac{f_{s_i}}{\varepsilon_{s_i}^e} \tag{5}$$

where f_s is the current stress in the reinforcement and ε_s^e is the elastic strain component (total strain net plastic strain).

The total nodal forces for the element, arising from plastic offsets, can then be calculated as the sum of the concrete and reinforcement contributions. These are added to prestrain forces arising from elastic prestrain effects and from nonlinear expansion effects (see Reference 8). The solution then proceeds according to the algorithm described in Reference 6.

Envelope of concrete plastic offsets

In the formulations being proposed, a critical requirement is to define and retain the plastic strains occurring in the concrete. These strain offsets must be definable for any arbitrary direction in the concrete continuum, even as principal strain directions undergo rotation.

A Mohr's circle construction provides a simple means of tracking the plastic offsets [see Fig. 2(b)]. Given the concrete plastic strains relative to the x, y axes (ε_{cx}^p, ε_{cy}^p, and $\gamma\varepsilon_{cxy}^p$), the plastic strains in the directions corresponding to the principal axes are as follows

$$\varepsilon_{c1}^p = \frac{\varepsilon_{cx}^p + \varepsilon_{cy}^p}{2} + \frac{\varepsilon_{cx}^p - \varepsilon_{cy}^p}{2}\cos 2\theta + \frac{\gamma_{cxy}^p}{2}\sin 2\theta \tag{6}$$

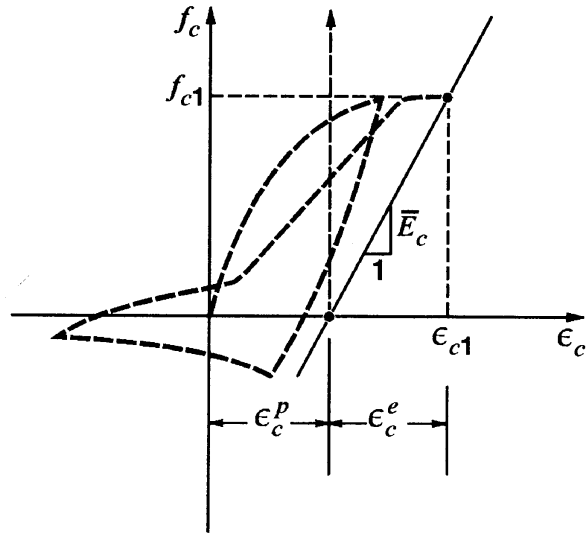

Fig. 1—Elastic and plastic components of concrete strain defined.

$$\varepsilon_{c2}^p = \frac{\varepsilon_{cx}^p + \varepsilon_{cy}^p}{2} - \frac{\varepsilon_{cx}^p - \varepsilon_{cy}^p}{2}\cos 2\theta - \frac{\gamma_{cxy}^p}{2}\sin 2\theta \tag{7}$$

The strains ε_{c1}^p and ε_{c2}^p are then used in the concrete constitutive models discussed later.

At any particular load step, further plastic straining may occur. Let $\Delta\varepsilon_{c1}^p$ and $\Delta\varepsilon_{c2}^p$ represent increments in the plastic strains in the principal directions; the increments may be positive or negative, regardless of whether the total strains are tensile or compressive. The parameters defining the envelope of plastic strains can be updated as follows

$$\varepsilon_{cx}^{p\prime} = \varepsilon_{cx}^p + \frac{\Delta\varepsilon_{c1}^p}{2}(1 + \cos 2\theta) + \frac{\Delta\varepsilon_{c2}^p}{2}(1 - \cos 2\theta) \tag{8}$$

$$\varepsilon_{cy}^{p\prime} = \varepsilon_{cy}^p + \frac{\Delta\varepsilon_{c2}^p}{2}(1 - \cos 2\theta) + \frac{\Delta\varepsilon_{c2}^p}{2}(1 + \cos 2\theta) \tag{9}$$

$$\gamma_{cxy}^{p\prime} = \gamma_{cxy}^p + \Delta\varepsilon_{c1}^p \cdot \sin 2\theta - \Delta\varepsilon_{c2}^p \cdot \sin 2\theta \tag{10}$$

Note that the principal direction θ is determined on the basis of the elastic strain components, not the total strains.

Envelopes of maximum concrete strains

In the hysteretic models for concrete stress that are typically used, stresses are calculated from sets of rules linked to a backbone curve. The latter is usually a formulation describing the monotonic response and requires the knowledge of the maximum concrete strains previously attained. In a continuum, where the principal strain directions may be rotating, this presents a complication.

Mohr's circle approach can again be used to approximately describe the maximum strains corresponding to an arbitrary direction. Consider first the maximum compressive strains in the concrete. Suppose, for the current load step, the principal elastic strains are ε_1^e, ε_2^e oriented in a direction θ relative to the reference axis x, y [see Fig. 2(a)]. The maximum compressive strains in the 1- and 2-directions, attained during previous loading, are given by

$$\varepsilon_{cm1} = \frac{\varepsilon_{cmx} + \varepsilon_{cmy}}{2} + \frac{\varepsilon_{cmx} - \varepsilon_{cmy}}{2} \cdot \cos 2\theta + \frac{\gamma_{cmxy}}{2} \cdot \sin 2\theta \tag{11}$$

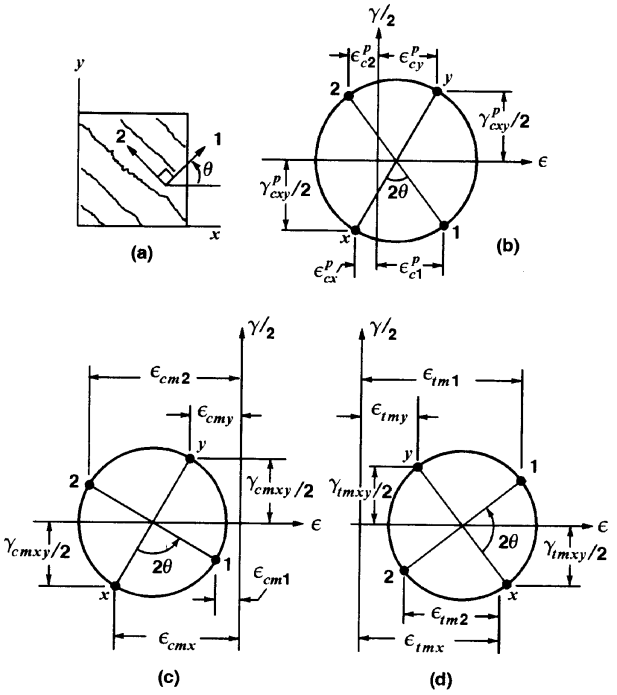

Fig. 2—Defining envelopes of maximum concrete strains: (a) principal axes in cracked element; (b) concrete plastic strains; (c) Mohr's circle for maximum compressive strains; and (d) Mohr's circle for maximum tensile strain.

$$\varepsilon_{cm2} = \frac{\varepsilon_{cmx} - \varepsilon_{cmy}}{2} + \frac{\varepsilon_{cmx} - \varepsilon_{cmy}}{2}\cos 2\theta - \frac{\gamma_{cmxy}}{2} \cdot \sin 2\theta \quad (12)$$

where ε_{cmx}, ε_{cmy}, and γ_{cmxy} are quantities defining maximum compressive strains relative to the x, y-axes and are used to define Mohr's circle in Fig. 2(c). The principal strains ε_{cm1} and ε_{cm2} are then used in defining the backbone curve for the compression response (discussed later).

If the current total compressive strains are greater than those previously recorded, then the maximum strain envelope must be updated. Thus, the strain increments $\Delta\varepsilon_{cm1}$ and $\Delta\varepsilon_{cm2}$ are defined as

$$\Delta\varepsilon_{cm1} = \begin{cases} 0 & \text{if } \varepsilon_1 > \varepsilon_{cm1} \\ \varepsilon_1 - \varepsilon_{cm1} & \text{if } \varepsilon_1 < \varepsilon_{cm1} \end{cases} \quad (13)$$

$$\Delta\varepsilon_{cm2} = \begin{cases} 0 & \text{if } \varepsilon_2 > \varepsilon_{cm2} \\ \varepsilon_2 - \varepsilon_{cm2} & \text{if } \varepsilon_2 < \varepsilon_{cm2} \end{cases} \quad (14)$$

The parameters defining the compressive strain envelope are then updated as follows

$$\varepsilon'_{cmx} = \varepsilon_{cmx} + \frac{\Delta\varepsilon_{cm1}}{2}(1 + \cos 2\theta) + \frac{\Delta\varepsilon_{cm2}}{2}(1 - \cos 2\theta) \quad (15)$$

$$\varepsilon'_{cmy} = \varepsilon_{cmy} + \frac{\Delta\varepsilon_{cm2}}{2}(1 - \cos 2\theta) + \frac{\Delta\varepsilon_{cm2}}{2}(1 + \cos 2\theta) \quad (16)$$

$$\gamma'_{cmxy} = \gamma_{cmxy} + \Delta\varepsilon_{cm1} \cdot \sin 2\theta - \Delta\varepsilon_{cm2} \cdot \sin 2\theta \quad (17)$$

An envelope for the maximum tensile strains in the concrete is developed in a similar manner [see Fig. 2(d)].

A total of six strain parameters (namely, ε_{cmx}, ε_{cmy}, γ_{cmxy}, ε_{tmx}, ε_{tmy}, and γ_{tmxy}) must be retained in memory for each integration point to adequately define the maximum concrete strains. Note that the Mohr's circles for maximum strain [Fig. 2(c) and 2(d)] do not represent a compatible strain condition present at any one time, but are a convenient means of keeping an approximate account of maximum strain in any one given direction.

CONCRETE STRESS-STRAIN MODELS

At the outset, it should be noted that the models presented herein are temporary and for demonstrative purposes only. For simplicity, essentially linear unloading/reloading rules are adopted. A comprehensive examination of currently available models and the development of improved formulations based on a extensive experimental investigation is currently underway.

First consider the compression response, illustrated in Fig. 3(a), occurring in either of the principal strain directions (i.e., $\varepsilon_c = \varepsilon_{c1}$ or $\varepsilon_c = \varepsilon_{c2}$; other parameters subscripted accordingly). The base curve describing the monotonic response is based on a Hognestad parabola or Popovics formulation, modified to account for compression softening effects according to the modified compression field theory (MCFT). The monotonic response curve is fully described in Reference 9.

On a reloading cycle where the concrete plastic strain in effect is ε_c^p, the concrete compressive stress is calculated as

$$f_c(\varepsilon_c) = \begin{cases} 0 & \text{if } \varepsilon_c > \varepsilon_c^p \text{ or } \varepsilon_c > 0 \\ (\varepsilon_c - \varepsilon_c^p)\dfrac{f_{cm}}{(\varepsilon_{cm} - \varepsilon_c^p)} & \text{if } \varepsilon_c^p > \varepsilon_c > \varepsilon_{cm} \\ f_{bc}(\varepsilon_c) & \text{if } \varepsilon_c < \varepsilon_{cm} \end{cases} \quad (18)$$

where ε_{cm} is the maximum compression strain attained during previous loading, in the direction in question; f_{cm} is the stress corresponding to ε_{cm}; and $f_{bc}(\varepsilon_c)$ is the stress calculated from the base curve for a strain ε_c. (Note: ε_c and ε_{cm} are total strains, plastic strains included.) If the response falls on the envelope curve (i.e., $\varepsilon_c < \varepsilon_{cm}$), then ε_{cm} and f_{cm} are updated to ε'_{cm} and f'_{cm}, respectively.

At each load stage, the instantaneous plastic strain $\varepsilon_c^{p\prime}$ is calculated as follows

$$\varepsilon_c^{p\prime} = \begin{cases} \varepsilon_c - \varepsilon_p\left[0.87\left(\dfrac{\varepsilon_c}{\varepsilon_p}\right) - 0.29\left(\dfrac{\varepsilon_c}{\varepsilon_p}\right)^2\right] & \text{if } \varepsilon_c > 1.5\varepsilon_p \\ \varepsilon_c - 0.001305\left(\dfrac{\varepsilon_p}{0.002}\right) & \text{if } \varepsilon_c < 1.5\varepsilon_p \end{cases} \quad (19)$$

where ε_p is the strain corresponding to the peak stress in the base curve (see Reference 9). If the instantaneous plastic strain exceeds the plastic offset ε_c^p, then the latter is updated accordingly.

Unloading at any time produces stresses according to the relationship

$$f_c(\varepsilon_c) = E_{cm}(\varepsilon_c - \varepsilon_c^p) \quad (20)$$

where unloading modulus E_{cm} is defined as

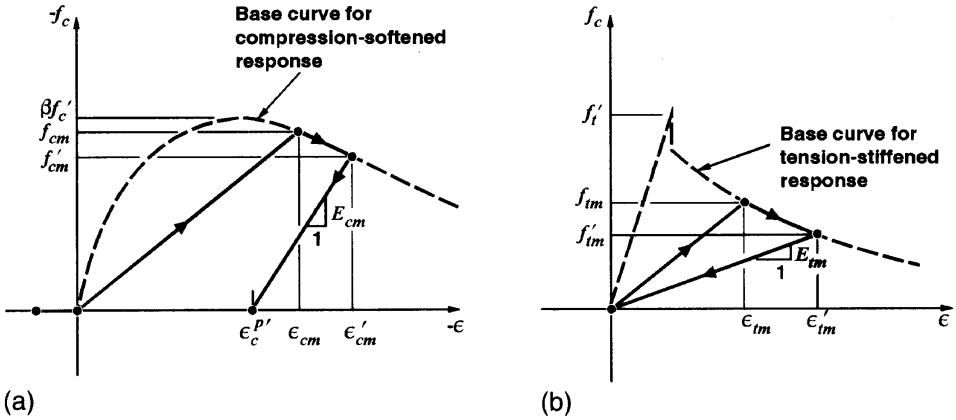

Fig. 3—Hysteresis models for concrete: (a) compression response; and (b) tension response.

$$E_{cm} = \frac{f_{cm}}{(\varepsilon_{cm} - \varepsilon_c^{p\prime})} \tag{21}$$

Implicit in this model is the assumption that, in an excursion returning from the tensile strain domain, the compressive stresses remain zero until the cracks completely close (i.e., until $\varepsilon_c < 0$). In fact, experimental evidence strongly suggests otherwise. The re-contact strain will be somewhat greater than zero and will be influenced by such factors as the crack shear slip. Modifications to the formulations can easily be implemented as they are developed.

Consider next the response in the tensile stress domain, illustrated in Fig. 3(b). The base curve consists of two parts: that describing the precracked response and that representing the postcracking tension-stiffened response. This base response is fully described in Reference 7.

On a reloading cycle, when the active plastic strain is ε_c^p, the concrete tensile stress is calculated as

$$f_c(\varepsilon_c) = \begin{cases} \dfrac{(\varepsilon_c - \varepsilon_c^p)}{(\varepsilon_{tm} - \varepsilon_c^p)} \cdot f_{tm} & \text{if } \varepsilon_c^p < \varepsilon_c < \varepsilon_{tm} \\ f_{bt}(\varepsilon_c) & \text{if } \varepsilon_c > \varepsilon_{tm} \end{cases} \tag{22}$$

where ε_{tm} is the maximum tensile strain attained during previous loading; f_{tm} is the stress corresponding to ε_{tm}; and $f_{bt}(\varepsilon_c)$ is the stress calculated from the base curve for a strain ε_c.

On the first tension cycle, the plastic offset ε_c^p is held constant at the value determined as response crosses from the compression domain. The strain then used in the base curve calculation is net of the plastic strain (i.e., the base curve is shifted such that its origin coincides with ε_c^p). In subsequent cycles, the plastic strain offset is redefined as follows

$$\varepsilon_c^{p\prime} = \begin{cases} \varepsilon_c & \text{if } \varepsilon_c^p < \varepsilon_c < 0 \\ 0 & \text{if } \varepsilon_c > 0 \end{cases} \tag{23}$$

Thus, no positive offsets are currently considered due to lack of a suitable model at the moment. The implication is that the tension response will pass through the origin during both loading and unloading.

When response falls on the envelope curve (i.e., $\varepsilon_c > \varepsilon_{tm}$), the maximum tensile strain and corresponding stress are updated to ε_{tm}' and f_{tm}', respectively [see Fig. 3(b)]. Stresses during unloading can be calculated from

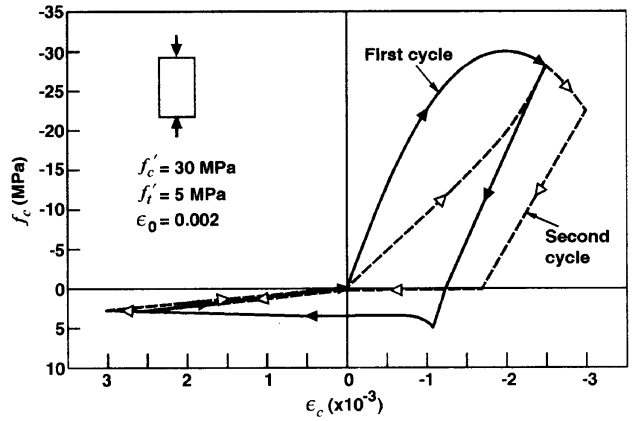

Fig. 4—Modeled response for element subjected to uniaxial strain excursions.

$$f_c(\varepsilon_c) = E_{tm}(\varepsilon_c - \varepsilon_c^p) \tag{24}$$

where unloading modulus E_{tm} is defined as

$$E_{tm} = \frac{f_{tm}'}{(\varepsilon_{tm}' - \varepsilon_c^p)} \tag{25}$$

To better illustrate the loading and unloading response obtained from the previously mentioned formulations, consider the response shown in Fig. 4. It relates to a reinforced concrete element subjected to a $\pm 2.5 \times 10^{-3}$ strain excursion through the first cycle, and a $\pm 3.0 \times 10^{-3}$ strain excursion through the second cycle. The material properties are as shown; the loading is uniaxial, and it is assumed that the reinforcement does not yield across the cracks (i.e., full tension stiffening is sustainable). It is worth noting that, during the second loading cycle in compression, the reloading curve is not quite linear. This occurs because the plastic offset is continually being redefined at each load step (a step size of 0.1×10^{-3} was used). The same effect leads to essentially zero tensile stresses during the second and subsequent cycles when $\varepsilon_c < 0$. It is recognized that the tension unloading and reloading curves passing through the origin and the absence of compressive stresses in the tensile strain domain are at odds with observed and accepted behavior. It is not a result of any limitations in the formulation approach, but due to lack of suitable models. Improved models can easily be adopted as they are developed.

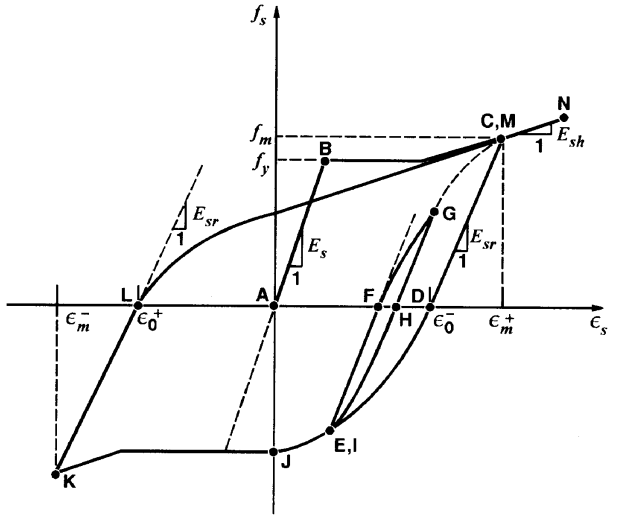

Fig. 5—Hysteresis model for reinforcement (adapted from Seckin[10]).

REINFORCEMENT STRESS-STRAIN MODELING

The monotonic stress-strain response is assumed to be trilinear. The initial stiffness of the reinforcement is E_s, giving way to a flat-top yield plateau when the yield stress f_y is reached. At a strain of ε_{sh}, a strain-hardening response with a stiffness of E_{sh} begins.

The reloading and hysteretic response of the reinforcement is modeled after Seckin[10] with some minor simplifications. The Bauschinger effect is represented by a Ramberg-Osgood formulation, as illustrated in Fig. 5. The first loading cycle is as per the monotonic response. Unloading at any time is given by

$$f_s(\varepsilon_i) = f_{s_{i-1}} + E_r(\varepsilon_i - \varepsilon_{i-1}) \quad (26)$$

where E_r is the unloading modulus (given below). The stresses upon reloading are given by

$$f_s(\varepsilon_i) = E_r(\varepsilon_i - \varepsilon_o) + \frac{E_m - E_r}{N \cdot (\varepsilon_m - \varepsilon_o)^{N-1}} \cdot (\varepsilon_i - \varepsilon_o)^N \quad (27)$$

where

$$N = \frac{(E_m - E_r)(\varepsilon_m - \varepsilon_o)}{f_m - E_r(\varepsilon_m - \varepsilon_o)} \quad (28)$$

and

$$E_r = \begin{cases} E_s & \text{if } (\varepsilon_m - \varepsilon_o) < \varepsilon_y \\ E_s\left(1.05 - 0.05\dfrac{\varepsilon_m - \varepsilon_o}{\varepsilon_y}\right) & \text{if } \varepsilon_y < (\varepsilon_m - \varepsilon_o) < 4\varepsilon_y \\ 0.85E_s & \text{if } (\varepsilon_m - \varepsilon_o) > 4\varepsilon_y \end{cases} \quad (29)$$

In a positive cycle, ε_m is the maximum positive strain attained during previous cycles, f_m is the stress corresponding to ε_m as determined from the backbone curve, and E_m is the tangent stiffness at ε_m. The parameter ε_o is the plastic offset strain corresponding to the zero stress point for the present cycle; it is redefined whenever the stress passes through zero. Note that the reloading curve is tangent to the unloading curve at $\varepsilon_i = \varepsilon_o$, and converges tangent to the backbone curve at $\varepsilon_i = \varepsilon_m$. The unloading stiffness E_r is dependent on the magnitude of the strain excursion relative to the yield strain ε_y.

In a negative cycle, the same formulations apply except that ε_m is the maximum negative strain previously attained. The stress f_m and stiffness E_m are evaluated accordingly. For the first reverse cycle (positive or negative), ε_m is taken as zero, with $f_m = f_y$ and $\varepsilon_m = 0$.

The model requires five parameters to be retained in memory for each reinforcement component at each integration point. These are the maximum positive and negative strains attained ε_m^+ and ε_m^-; the reinforcement stress and strain from the previous load step $f_{s_{i-1}}$ and ε_{i-1}; and the zero point strain ε_o.

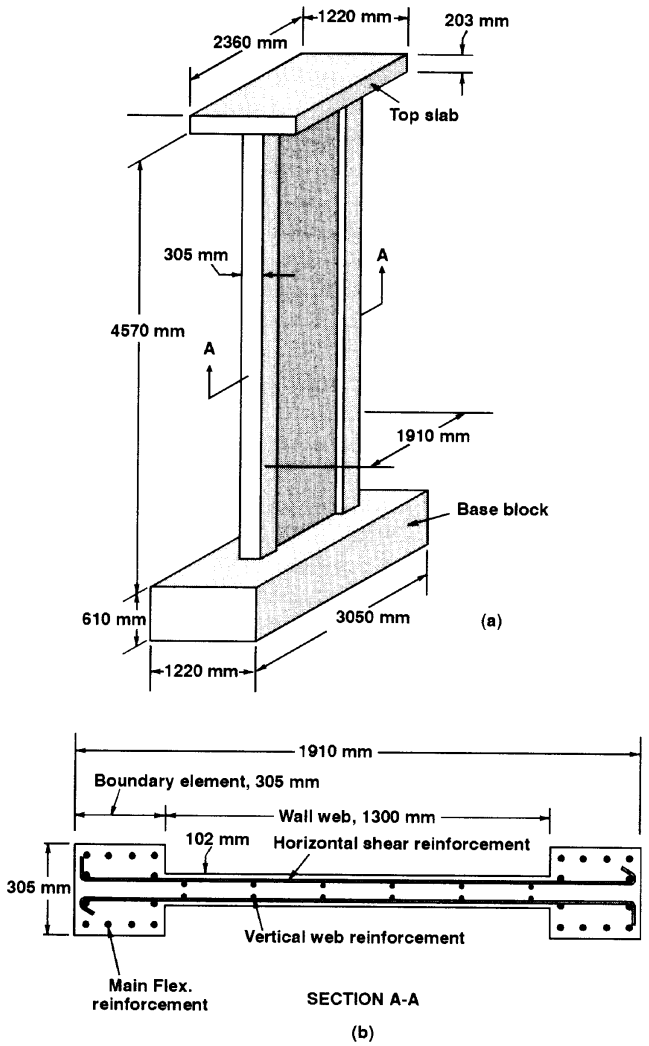

Fig. 6—Details of PCA Wall B2, taken from Oesterle et al.[12]

ANALYSIS OF SHEARWALL

To obtain a preliminary indication of the suitability of the proposed approach to cyclic response modeling of reinforced concrete, an analysis of a large-scale shearwall structure was undertaken. The structure chosen for investigation was Wall B2.[11] The series of wall tests that included this specimen is widely regarded as a benchmark against which theoretical formulations are calibrated. Wall B2 was a barbell-shaped wall, measuring 1910 mm (6 ft 3 in.) in total width and 4670 mm (15 ft) in height from the base (Fig. 6). The wall web was 102-mm (4-in.) thick, and contained 0.63 percent horizontal reinforcement and 0.29 percent vertical reinforcement. The thickened boundary elements were 305 mm (12 in.) square and contained 3.67 percent vertical reinforcement. The wall was built integral with a heavy base structure and stiff top slab. The

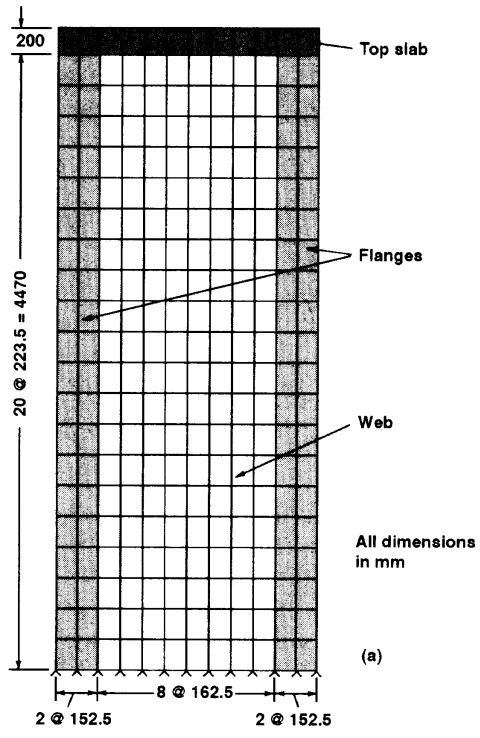

Zone	Thickness (mm)	Concrete f'_c (MPa)	Concrete E_c (MPa)	Horizontal Reinforcement ρ (%)	Horizontal Reinforcement f_y (MPa)	Vertical Reinforcement ρ (%)	Vertical Reinforcement f_y (MPa)
I (Web)	102	53.7	32 700	0.63	533	0.29	533
II (Flanges)	305	53.7	32 700	0.63	533	3.67	410
III (Top Slab)	1220	53.7	32 700	3.00 *	600 *	3.00 *	600 *

E_s = 200 000 MPa
E_{sh} = 2 000 MPa
ϵ_{sh} = 5.0 x 10^{-3}
* Assumed
(b)

Fig. 7—Finite element mesh used to model Shearwall B2.

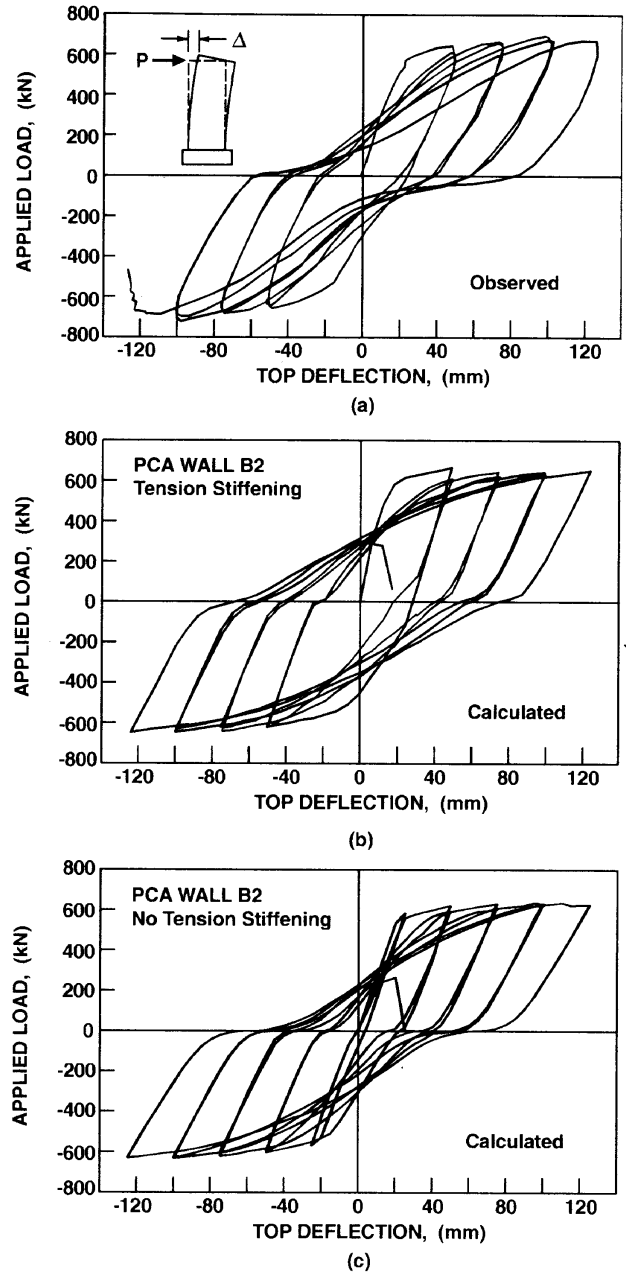

Fig. 8—Response of Shearwall B2: (a) experimentally measured response; (b) predicted response assuming no decay in tension stiffening; and (c) predicted response assuming full decay in tension stiffening.

top slab was subjected to lateral cyclic displacements progressively increasing in magnitude, eventually leading to a concrete crushing failure in the web. The shear-dominated behavior of the wall represents a stringent test of the analysis procedures.

Wall B2 was modeled using the finite element mesh shown in Fig. 7, comprising 252 linear displacement rectangular elements. The mesh is divided into three zones, representing the web portion, the flanges, and the top slab, respectively. Reinforcement details and material properties for each zone are also given in Fig. 7. The material properties, and other pertinent details, used in modeling the structure were as reported by Sittipunt and Wood.[3] Note that the wall is assumed fully fixed at the base, and no attempt is made to model bond slip. Loading history was imposed by specifying lateral displacements at the top center node of the top slab.

An initial analysis was done assuming no further deterioration in the compression softening and tension stiffening responses, due to cyclic loading, than is currently assumed by the MCFT for monotonic loading. The imposed loading consisted of two cycles of top lateral deflection at each amplitude level, beginning at ±75-mm (3-in.) amplitude and increasing by 25 mm until failure occurred. The resulting predicted response is shown in Fig. 8(b), compared to the experimentally observed response shown in Fig. 8(a). The correlation is reasonably good in the following respects: 1) the wall's lateral resistance is approximately 625 kN; 2) there is only a minor increase in lateral resistance with increasing displacement amplitude beyond ±75 mm, that is, the envelope of response in nearly flat-top; 3) failure occurs during the ±125-mm excursion, although in the predicted response, it occurred at the start of the second +125-mm cycle, whereas in the experiment failure it occurred towards the peak of the first -125-mm cyclic; 4) failure is characterized by crushing of the concrete web near the base region; 5) residual deflections upon unloading are significant and cumulative, indicating a racheting effect occurring in the vertical reinforcement in the flanges; and 6) the lateral stiffness of the wall is progressively diminishing. The only notable discrepancy between calculated and observed behavior is the degree of pinching evident in the load-deflection hysteresis. This is likely related to the shape of the base hysteretic models used for the compression and tension responses, and to an overestimation in tension stiffening effects. Other mechanisms, such as cyclic shear slip along the crack surfaces due to deterioration in aggregate interlock, also contribute to the pinched nature of the observed response.

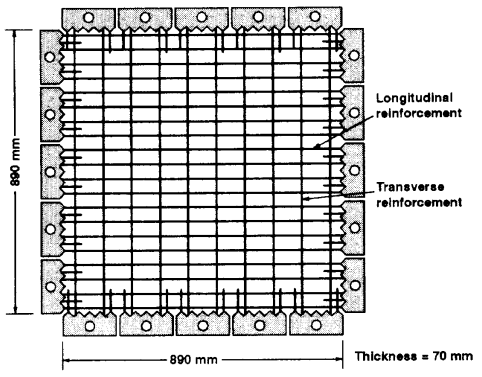

(a)

Panel	PDV1	PDV2	PDV3
f'_c (MPa)	26.8	23.7	34.1
ϵ_0 ($\times 10^{-3}$)	1.62	1.63	1.69
ρ_x (%)	1.82	1.82	1.82
f_{yx} (MPa)	282	282	282
ρ_y (%)	0.91	0.91	0.91
f_{yy} (MPa)	282	282	282
Loading	Monotonic	Reversed cyclic	Cyclic

(b)

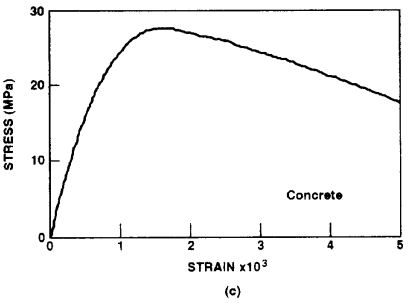

(c)

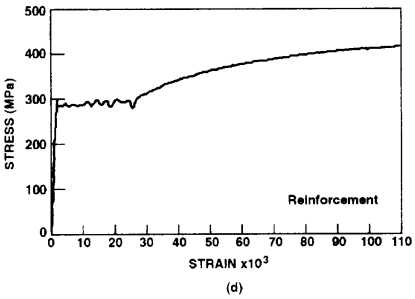

(d)

Fig. 9—Details of PDV series of panel tests: (a) specimen layout; (b) test parameters; (c) concrete cylinder response; and (d) reinforcement coupon response.

Stevens et al.[4] observed from panel tests that the tension stiffening effect diminishes significantly as a result of cyclic loading. To investigate the significance of this factor, the analysis of Wall B2 was repeated, assuming no tension stiffening effects (i.e., no postcracking tensile stresses in the concrete). The resulting load-deflection is shown in Fig. 8(c). Note that the hysteretic response is somewhat more pinched than previously and is a closer match to the experimental behavior. Other aspects of the correlation to the experimental response remain strong, including the load capacity, failure mode, stiffness response, and residual deflection.

It should be noted that the analysis algorithms were highly stable and quick to converge at each load stage. The indication from this analysis is that the proposed approach to modeling cyclic load effects is a viable one.

PANEL TESTS

Analysis of structures such as the shearwall previously discussed are helpful in testing the ability of a calculation procedure to model complex behaviors and interactions in structures. However, the data most valuable in assessing the fundamental constitutive behavior of reinforced concrete, under various conditions including cyclic loading, is that obtained from simple elements subjected to well-defined and well-controlled loads.

As previously noted, Stevens et al.[4] subjected three large-scale panel elements to reversed cyclic load conditions. Among their findings were that "reversed cyclic loading under biaxial conditions results in a reduction of the peak compressive stress in excess of that observed for monotonic loading." They also observed reductions in the postcracking tensile stresses in the concrete as a result of cyclic loading. Some constitutive relations were formulated accordingly, although not in a form useful for this study.

To build on the work of Stevens, a more comprehensive series of panel tests is planned. The objective of the work is to accumulate the necessary data to more accurately define hysteretic models for cracked reinforced concrete in compression and in tension, under general loading conditions. The pilot series for this program involved three 890 x 890 x 70-mm orthogonally-reinforced panels; namely Panels PDV-1, PDV-2, and PDV-3.[13] The panels were constructed of normal strength concrete and contained 1.82 percent reinforcement in one direction and 0.91 percent reinforcement in the perpendicular direction (x- and y-directions, respectively). The reinforcement was fabricated from deformed D5 bar, with a nominal diameter of 6.0 mm. Details of the specimen construction and material properties are provided in Fig. 9(a) and (b). Typical stress-strain response curves for the concrete and reinforcement are provided in Fig. 9(c) and (d), respectively.

The test panels were loaded under conditions of biaxial compression and shear in the fixed proportion of fn_x:fn_y:v = -0.4:-0.4:1.0. Panel PDV-1 was subjected to monotonically increasing load; Panel PDV-3 was subjected to cyclic loading (unidirectional, with unloading to zero between cycles); and Panel PDV-2 was subjected to reversed cyclic shear. Loads were applied in equal increments of v = 0.5 MPa per load stage up until approximately 70 percent of ultimate capacity, then at increments of 0.25 MPa thereafter.

All three panels failed by shear failure of the concrete occurring almost coincidently with yielding of the reinforcement in the x-direction. The reinforcement in the y-direction typically yielded well before failure. The state of the panels at failure are shown in Fig. 10; Fig. 11 gives the measured shear stress-strain response curves. In comparing the response of PDV-2 with that of control panel PDV-1, it is reasonable to surmise that the effect of cyclic load was to cause significant further deterioration in the strength and stiffness of the concrete. Note that in comparing ultimate loads, it is important to consider that the strength of the concrete for PDV-3 was significantly higher than in the other two panels.

The test panels were analyzed with the finite element procedure discussed previously. In all cases, it was found that the strength of the panels was governed by yielding of the reinforcement in both directions. The large strains accompanying the yielding subsequently led to concrete shear failures. The predicted load-deformation responses are shown in Fig. 12. In the case of the monotonically loaded panel (PDV-1), the correlation between experimental and calculated response is good in all respects. In the cyclic and reversed-cyclic panels, some disparities become evident. The experimental responses demonstrate a behavior more influenced by concrete shear failure, with substantially lower stiffness and significantly different residual strains upon unloading. The clear indication is that the damage to the concrete is more extensive than that assumed in the models. This becomes more clear when we examine the

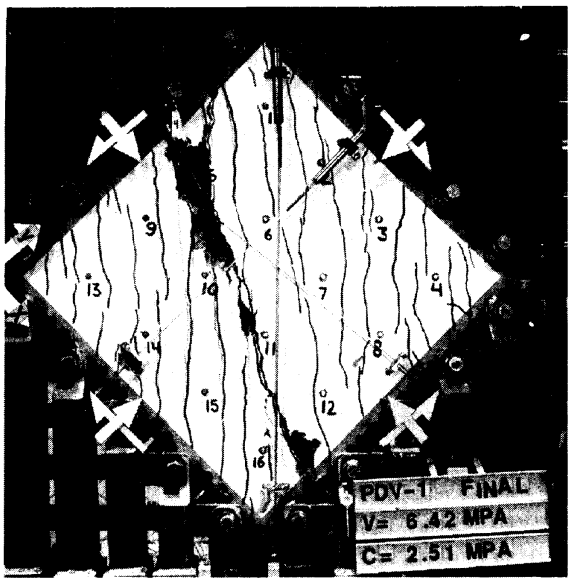

(a)

(b)

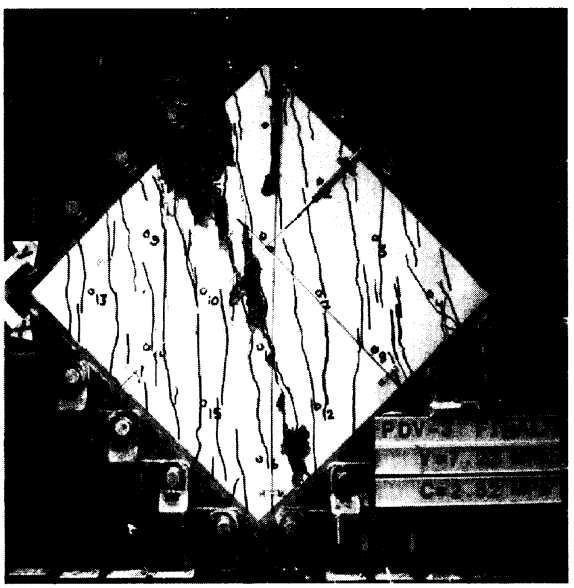

(c)

Fig. 10—Test panels at failure: (a) Panel PDV-1 subjected to monotonic loading; (b) Panel PDV-2 subjected to reversed cyclic loading; and (c) Panel PDV-3 subjected to cyclic loading.

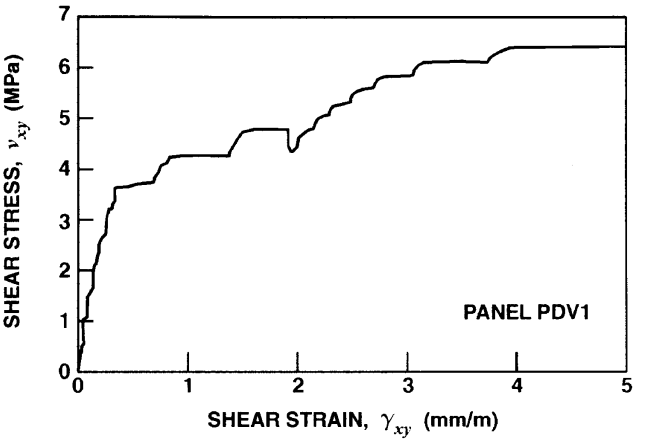

(a)

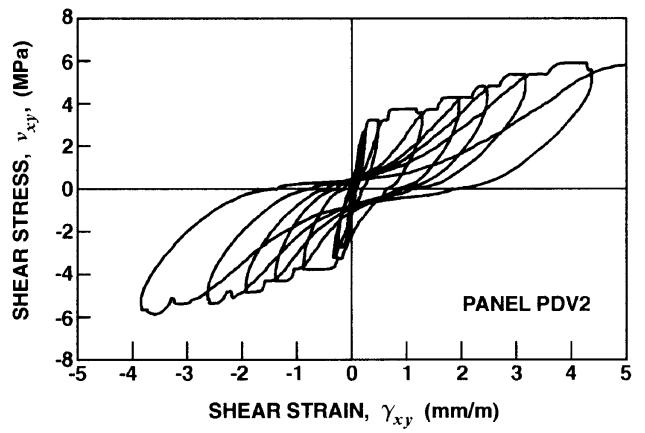

(b)

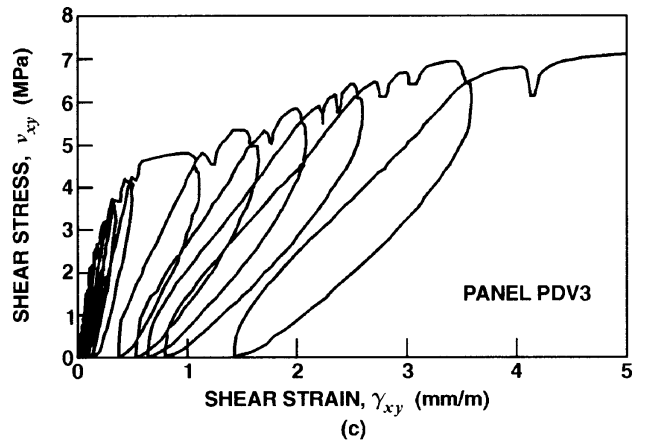

(c)

Fig. 11—Measured shear stress-strain response of test panels: (a) Panel PDV-1; (b) Panel PDV-2; and (c) Panel PDV-3.

principal compressive and principal tensile stress-strain behaviors. Shown in Fig. 13 are the calculated and observed compression responses of Panel PDV-2 for the first $v = 5.0$ MPa cycle. The inadequacy of the hysteretic models is clearly evident.

Thus, the nonlinear hysteric models for concrete subjected to cyclic loads are critical to properly modeling the response. Their influence may not be so apparent when examining macroscopic behavior in structures such as shearwalls, where behavior is largely influenced by reinforcement yielding. However, it can be significant in correctly predicting localized damage, failure modes, and failure loads in shear or compression critical structures.

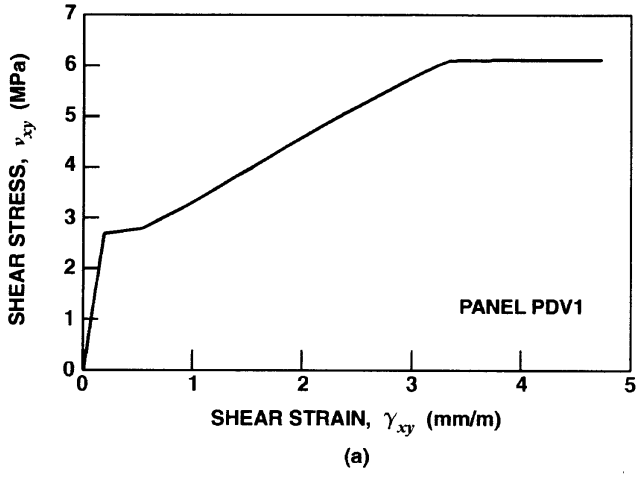

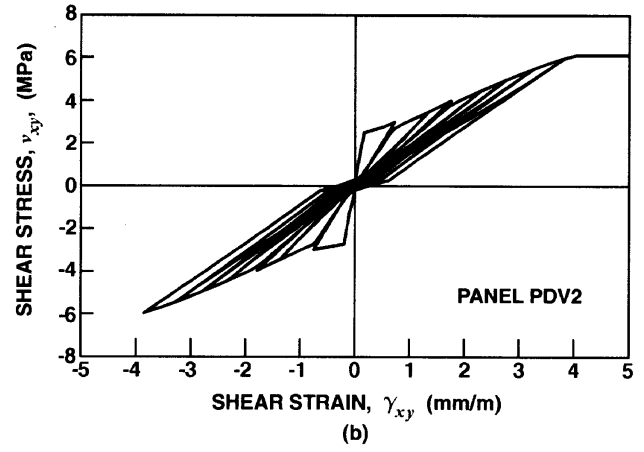

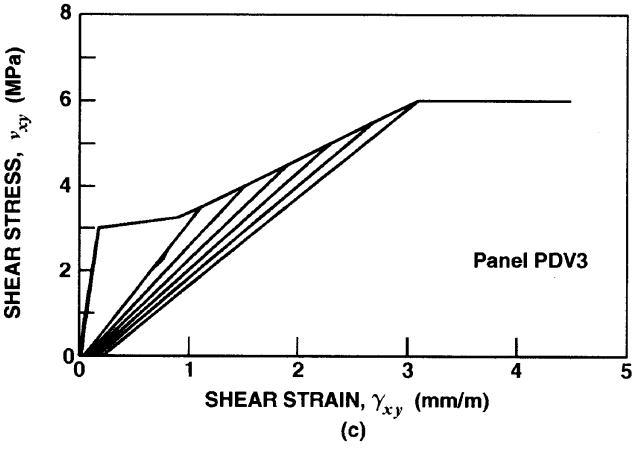

Fig. 12—Calculated shear stress-strain response of test panels: (a) Panel PDV-1; (b) Panel PDV-2; and (3) Panel PDV-3.

CONCLUSIONS

From the previous discussions, the following conclusions can be drawn:

1. Employing strain offsets to model the plastic components of strain in the concrete and reinforcement leads to a viable means of using secant stiffness-based procedures for modeling reversed cyclic load effects in reinforced concrete structures.

2. The resulting analysis procedure exhibits excellent convergence and numerical stability characteristics.

3. A Mohr's circle approach is useful for constructing envelopes defining the plastic strain offset, the maximum compressive strain, and the maximum tensile strain sustained by the concrete, in any particular direction, as a result of previous loading.

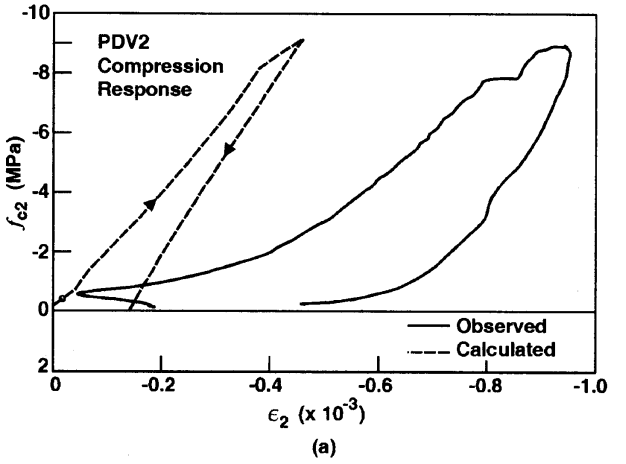

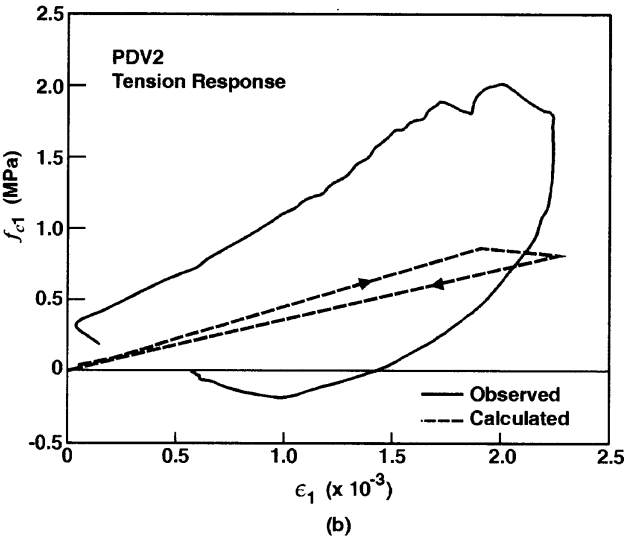

Fig. 13—Comparison of measured and calculated concrete stresses for Panel PDV-2 during first v = *5.0 MPa cycle: (a) principal compressive stresses; and (b) principal tensile stresses.*

4. A constitutive modeling approach based on a smeared rotating crack assumption eliminates the need for separate hysteretic models for normal stress and shear stress response of the concrete. Rather, the concrete can more conveniently be modeled as a nonlinear orthotropic material in the conventional sense, with relations expressing the principal compressive and principal tensile stress behavior.

5. The load-deformation response of many reinforced concrete structures, such as the shearwall examined, is dominated by the reinforcement behavior, even though ultimate load and failure mode may be governed by the concrete. Proper modeling of the Bauschinger effect in the reinforcement plays a large part in accurately simulating the structure's behavior.

6. Localized behavior, load capacity, and failure mode may, in some cases, be strongly influenced by the highly nonlinear hysteretic response of the concrete. Simple linear unloading and reloading rules do not adequately represent response and prevent the analysis procedure from capturing important subtleties in behavior. In particular, the inability of cracks to completely close before compression response begins is an important factor.

Experimental work is currently underway to define additional damage factors for concrete subjected to repeated cyclic loads, both for further softening of the concrete in compression and for the shake-out of stress in tension. In addition, the experimental work will lead to the formulation of more realistic unloading-reloading models useful in a smeared rotating crack context. These refined models can then be easily implemented using the plastic offset method described.

NOTATION

E_c = initial stiffness modulus of concrete
$\tilde{E}_c$ = secant stiffness modulus of concrete
E_{cm} = *unloading modulus for concrete in compression*
E_r = unloading modulus for reinforcement
E_s = initial stiffness modulus for reinforcement
$\tilde{E}_s$ = secant stiffness modulus for reinforcement
E_{sh} = strain hardening modulus for reinforcement
E_{tm} = unloading modulus for concrete in tension
f_{bc} = concrete stress calculated from base curve
f_c = normal stress in concrete
f'_c = concrete cylinder compressive strength
f_{cm} = concrete stress corresponding to maximum compressive strain
f_s = stress in reinforcement
f_{tm} = concrete stress corresponding to maximum tensile strain
f_y = yield stress of reinforcement
α = orientation of reinforcement, clockwise from reference x-axis
ε_1 = first principal strain in concrete
ε_2 = second principal strain in concrete
ε_c = total normal strain in concrete in given direction
ε^e_{ci} = elastic component of concrete strain in i-direction
ε^p_{ci} = plastic component of concrete strain in i-direction
ε_{cm_i} = maximum compression strain in i-direction
ε_o = strain at peak compressive stress in concrete cylinder
ε_p = strain corresponding to peak stress in concrete base curve
ε^e_{si} = elastic component of strain in reinforcement
ε^p_{si} = plastic component of strain in reinforcement
ε_{sh} = strain in reinforcement at which strain hardening begins
ε_{tm_i} = maximum tensile strain in concrete in i-direction
γ^p_{cxy} = plastic shear strain in concrete relative to x,y-axes
γ_{cmxy} = shear strain associated with maximum compressive strains in concrete
γ_{tmxy} = shear strain associated with maximum tensile strains in concrete
θ = orientation of principal strain directions, relative to x-axis

REFERENCES

1. "Finite Element Analysis of Reinforced Concrete II," *Proceedings*, International Workshop, ASCE, New York, 1993, 717 pp.

2. Okamura, H., and Maekawa, K., *Nonlinear Analysis and Constitutive Models of Reinforced Concrete*, Giho-do Press, University of Tokyo, Tokyo, 1991, 182 pp.

3. Sittipunt, C., and Wood, S. L., "Influence of Web Reinforcement on the Cyclic Response of Structural Walls," *ACI Structural Journal*, V. 92, No. 6, Nov.-Dec. 1995, pp. 745-756.

4. Stevens, N. J. et al., "Analytical Modeling of Reinforced Concrete Subjected to Monotonic and Reversed Loadings," *Publication* No. 87-1, Department of Civil Engineering, University of Toronto, Toronto, 1987.

5. Vecchio, F. J., "Nonlinear Finite Element Analysis of Reinforced Concrete Membranes," *ACI Structural Journal*, V. 86, No. 1, Jan.-Feb. 1989, pp. 26-35.

6. Vecchio, F. J., "Reinforced Concrete Membrane Element Formulations," *Journal of Structural Engineering*, ASCE, V. 116, No. 3, Mar. 1990, pp. 730-750.

7. Vecchio, F. J., and Collins, M. P., "The Modified Compression Field Theory for Reinforced Concrete Elements Subjected to Shear," ACI JOURNAL, *Proceedings* V. 83, No. 2, Mar.-Apr. 1986, pp. 219-231.

8. Vecchio, F. J., "Finite Element Modeling of Concrete Expansion and Confinement," *Journal of Structural Engineering*, ASCE, V. 118, No. 9, Sept. 1992, pp. 2390-2406.

9. Vecchio, F. J., and Collins, M. P., "Compression Response of Cracked Reinforced Concrete," *Journal of Structural Engineering*, ASCE, V. 119, No. 12, Dec. 1993, pp. 3590-3610.

10. Seckin, M., "Hysteretic Behaviour of Cast-in-Place Exterior Beam-Column-Slab Subassemblies," PhD thesis, Department of Civil Engineering, University of Toronto, 1981.

11. Oesterle, R. G. et al., "Earthquake-Resistant Structural Walls—Tests of Isolated Walls," *Report* to the National Science Foundation, Construction Technology Laboratories, Portland Cement Association, Skokie, Ill., Nov. 1976, 315 pp.

12. Oesterle, R. G. et al., "Web Crushing of Reinforced Concrete Structural Walls," ACI JOURNAL, *Proceedings* V. 81, No. 3, May-June 1984, pp. 231-241.

13. Villani, D. R., "Reinforced Concrete Subjected to Cyclic Loads: A Pilot Study," BASc thesis, Department of Civil Engineering, University of Toronto, 1995, 147 pp.